Journal of Solid State Chemistry **168,** 639–652 (2002)
doi:10.1006/jssc.2002.9762

Recent Advances in Fullerene Superconductivity

Serena Margadonna*[,1] and Kosmas Prassides†[,1]

*Department of Chemistry, University of Cambridge, Lensfield Road, Cambridge CB2 1EW, UK; and †School of Chemistry, Physics and Environmental Science, University of Sussex, Brighton BN1 9QJ, UK

Received January 28, 2002; in revised form May 1, 2002; accepted May 4, 2002

Superconducting transition temperatures in bulk chemically intercalated fulleride salts reach 33 K at ambient pressure and in hole-doped C_{60} derivatives in field-effect-transistor (FET) configurations, they reach 117 K. These advances pose important challenges for our understanding of high-temperature superconductivity in these highly correlated organic metals. Here we review the structures and properties of intercalated fullerides, paying particular attention to the correlation between superconductivity and interfullerene separation, orientational order/disorder, valence state, orbital degeneracy, low-symmetry distortions, and metal–C_{60} interactions. The metal–insulator transition at large interfullerene separations is discussed in detail. An overview is also given of the exploding field of gate-induced superconductivity of fullerenes in FET electronic devices.

Key Words: **superconductivity; fullerenes; metal–insulator transition; magnetism.**

1. INTRODUCTION

The fullerene family represents a new molecular form of pure carbon, which has proven to be of remarkable interest for both its chemical and physical properties. Following the serendipitous discovery of C_{60} (a quasi-spherical molecule with dimensions of ~ 1 nm) and the production of bulk crystalline samples of fullerenes from arc-processed carbon, research on the solid-state properties of fullerene-based nanostructures and nanonetworks has proceeded at an exhilarating pace (1). Novel carbon materials like the nanotubes, the buckyonions and the endohedral metallofullerenes have been subsequently discovered, while fullerene derivatives show a plethora of interesting properties, ranging from superconductivity to ferromagnetism and promise future applications in batteries, transistors and sensors among others.

[1] To whom correspondence should be addressed. Fax: +44-12-73-67-7196. E-mail: sm413@hermes.cam.ac.uk, k.prassides@sussex.ac.uk.

The most well-known derivatives of C_{60} are those with alkali metals, which become superconducting with high transition temperatures (up to 33 K at ambient pressure (2), rising to 40 K at high pressure (3)). Changing the size and nature of the dopants affects sensitively the superconducting properties of the materials (4), culminating in the recent observation of high temperature superconductivity at 117 K in hole-doped C_{60} derivatives (5). Another remarkable discovery has been the reaction of C_{60} with the strong organic donor tetrakis(dimethylamino)ethylene, (TDAE), resulting in the formation of a ferromagnetic solid, $(TDAE)C_{60}$, with a 16 K Curie temperature (6). Finally, an unexpected discovery in this field has been the ease with which C_{60} units can bond together, giving rise to polymerized fullerene networks with novel structural architectures. Such fullerene-bridged arrays display varying dimensionality and diverse types of bonding, also leading to fascinating electronic and magnetic properties. For instance, a two-dimensional (2D) polymeric form of C_{60} was reported to be ferromagnetic above room temperature (7). These results have ensured that a vigorous research effort in fullerene research will continue to be maintained in the foreseeable future.

2. INTERCALATED FULLERIDES

The high electron affinity of C_{60} and the weak intermolecular van der Waals forces between the molecules in the crystal make it an excellent potential host for reductive intercalation chemistry. Indeed, intercalation of solid C_{60} with electron donors, like the alkali metals, results in a wealth of intercalated fulleride salts with stoichiometries A_xC_{60}, where x can be as low as 1 (CsC_{60}) or as high as 12 ($Li_{12}C_{60}$). This reflects the ease of reduction of C_{60}, especially to oxidation states ranging from -1 to -6.

Metallic compositions are primarily encountered for stoichiometries A_3C_{60}. These salts are superconducting with T_c's as high as 33 K (at ambient pressure) for

0022-4596/02 $35.00

$RbCs_2C_{60}$ (2). The superconducting phases adopt, in general, either face-centered-cubic (fcc) or primitive cubic structures, in which the three cations occupy the available octahedral and tetrahedral interstitial sites. Charge transfer is essentially complete and the conduction band of C_{60}, which arises from its lowest unoccupied molecular orbital (LUMO) of t_{1u} symmetry is half filled (Fig. 1). The fullerides are potentially simpler materials than the high-T_c cuprates and thus perhaps more easily amenable to theoretical modelling; still they do pose many challenges, principally arising from the comparable magnitudes of the Fermi and phonon energies and the role of electronic correlations. Superconductivity has been explained by both conventional electron–phonon (8) and purely electronic (9) models. In both models, pair binding is assumed to be dominated by intramolecular properties. Experimental evidence derived from the relationship between lattice dimensions (i.e., interfullerene spacing) and superconducting transition temperatures (Fig. 2) in A_3C_{60} both at ambient and at high pressures is consistent with T_c being modulated by the density-of-states at the Fermi level, $N(\varepsilon_F)$ (4). As the interfullerene spacing increases, the overlap between the molecules decreases; this leads to a reduced bandwidth, and, for a fixed band filling, to an increased density of states. From a BCS-type relationship:

$$T_c \propto (\hbar\omega_{ph}) \exp[-1/N(\varepsilon_F)V] = (\hbar\omega_{ph}) \exp(-1/\lambda), \quad [1]$$

where V is the electron–phonon coupling strength, $\lambda = VN(\varepsilon_F)$, and ω_{ph} is the average intramolecular phonon energy, the observed T_c may be understood in terms of (i) a high average phonon frequency, $\hbar\omega_{ph}$, resulting from the light carbon mass and the large force constants associated with the intramolecular modes, (ii) a moderately large V with contributions from both radial and tangential C_{60} vibrational modes, and (iii) a high DOS at ε_F, resulting from the weak intermolecular interactions.

The role of electron correlations is a crucial ingredient in all attempts to understand the normal and superconducting state properties of A_3C_{60} fullerides, as the on-site Coulomb repulsion, U is comparable to or greater than the t_{1u} bandwidth, W. Estimates of U for the C_{60} molecule are of the order of 3 eV. This value is reduced in the solid and is generally assumed to be ≈ 1 eV. As typical values of W for A_3C_{60} are of the order of 0.5 eV, the ratio (U/W) is typically much larger than 1 whence the t_{1u} band should split into two and, as a result, a Mott–Hubbard insulator should be observed (10). For this reason, it was suggested

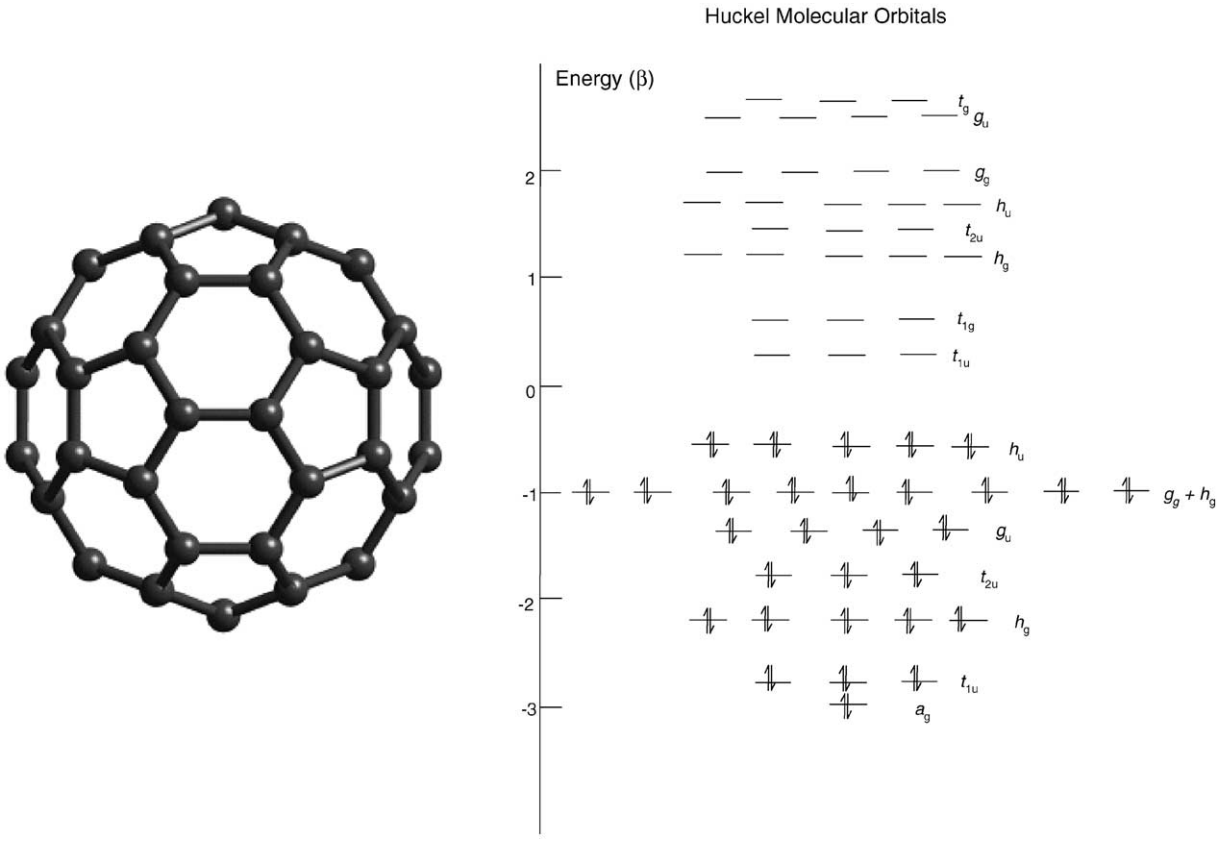

FIG. 1. The C_{60} molecule (left) and its corresponding molecular orbital energy level scheme.

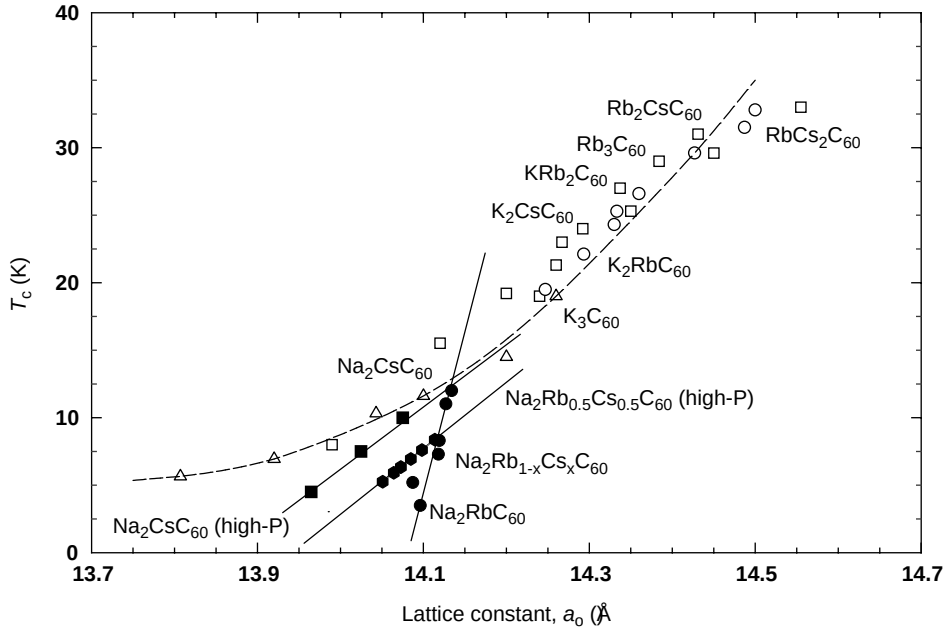

FIG. 2. Variation of T_c (K) with lattice parameter, a_0 (Å) for various compositions of A_3C_{60} and $Na_2A'C_{60}$ ($A' = Rb, Cs$). The dotted line is the T_c–a relationship expected from BCS theory using $N(\varepsilon_F)$ values obtained by LDA calculations, while the straight lines are guide to the eye.

that the metallic and superconducting behavior in A_3C_{60} arises through the effect of non-stoichiometry, namely the true composition is $A_{3-\delta}C_{60}$(11). However, the boundary of the metal–insulator transition shifts to a critical value of $(U/W)_c = 2.5$ when the triple orbital degeneracy of the LUMO states is taken into account, thus naturally accounting for the highly correlated metallic behavior of stoichiometric A_3C_{60} (10).

Highly doped states of C_{60}^{n-} ($n > 6$) can be synthesized when alkaline earth metals are used as intercalants. In such cases, the conduction band derives from the next unoccupied molecular orbital (LUMO + 1) of C_{60}, which is also triply degenerate with symmetry t_{1g} (Fig. 1). Partial occupancy of the t_{1g} orbitals can also lead to certain compositions, which display superconductivity. Recent studies have revealed that the behavior of alkaline earth fullerides cannot be directly extrapolated from that of their alkali fulleride antecedents (12). For example, while non-cubic A_4C_{60} fullerides are insulating, Ba_4C_{60} and Sr_4C_{60} are bulk superconductors with $T_c = 6.7$ and 4.4 K, respectively, despite possessing a non-half-filled conduction band and adopting highly anisotropic orthorhombic structures.

2.1. The Parent Superconducting Fullerides K_3C_{60} and Rb_3C_{60}

The structure of the parent A_3C_{60} ($A = K, Rb$) fullerides is fcc and is based on the cryolite structural type (Fig. 3) (13). If we consider the size of the two interstitial sites for intercalation, we can see that the octahedral one (radius ≈ 2.06 Å) is large enough to accommodate all alkali metal ions, while the tetrahedral one (radius ≈ 1.12 Å) has a size larger than Na^+ but smaller than K^+. As a result, the size of the alkali ions occupying the tetrahedral voids plays a crucial role in determining the structural properties of alkali fullerides and ions larger than Na^+ cannot be accommodated without substantial expansion of the lattice. Thus, different structural behaviors are observed between alkali fullerides containing large alkali ions (Cs, Rb, K) and those containing the smaller Na^+ or Li^+.

In the first case, the structure is best described in the space group $Fm\bar{3}m$ with a unit-cell size larger than that of C_{60} (14.24 Å for K_3C_{60}) (13). The fulleride ions are no longer free to rotate, as in the case of pure C_{60}, due to steric effects associated with the alkali ions in the tetrahedral sites. Instead, they are characterized by merohedral disorder and occur in two equally populated orientations related by a 90° rotation about the [001] or equivalently by 44°23' about the [111] crystal axis. No phase transitions driven by changes in the reorientational behavior occur as a function of temperature or pressure. The C_{60}^{3-} ions perform small-amplitude librational motion whose amplitude increases and energy decreases with increasing temperature. The crystal structure is well understood in terms of the strong repulsive interactions between the alkali ions and the fulleride units. The latter are forced to expose towards the tetrahedral alkali ions the part of their quasi-spherical shape with the largest surface area, namely the

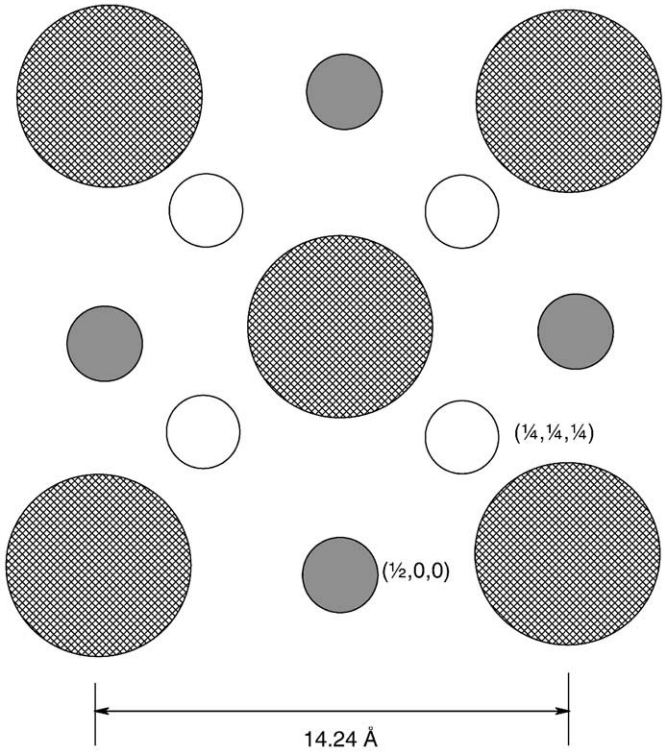

FIG. 3. The cryolite structural type adopted by K_3C_{60}. The shaded and open spheres represent potassium ions residing in the octahedral and tetrahedral sites, respectively.

hexagonal faces, thus leading to maximization of the A^+–$C(C_{60})$ distances. The resulting alkali metal coordination geometry is to four hexagonal faces of neighboring fulleride ions (tetrahedral site, coordination number 24) and to six hexagon–hexagon (6:6) fusions (octahedral site, coordination number 12).

Despite the apparent simplicity of the A_3C_{60} structure, some important issues are not as yet fully resolved. One feature of the structural data is the large isotropic temperature factor found for the octahedral ion (~ 16 Å^2), implying the existence of substantial static and/or dynamic disorder (13). In addition, while the crystal structure is consistent with the presence of only two inequivalent alkali ions, ^{39}K and ^{87}Rb NMR measurements in K_3C_{60} and Rb_3C_{60} reveal that the peak associated with the tetrahedrally coordinated ions splits into two components (T and T') at low temperature (14). Possibilities to account for this behavior include the existence of local misorientations of C_{60}^{3-} ions, displacement of the octahedral ions off the center of the interstices, molecular Jahn–Teller distortions, structural instabilities like charge density waves, or a small concentration δ of tetrahedral vacancies. Careful analysis of synchrotron X-ray diffraction data has provided support for the presence of such tetrahedral vacancies in $K_{3-\delta}C_{60}$ with $\delta \approx 0.07$ (15).

2.2. Alkali Fullerides with Small Interfullerene Separations

2.2.1. Sodium Fullerides

The control of the structural properties of intercalated fullerides by the ion occupying the tetrahedral interstices is immediately evident when Na^+ is introduced in the tetrahedral holes of a cubic-close-packed (ccp) array of C_{60}^{3-} ions. For instance, in Na_2CsC_{60} (16), the C_{60}^{3-} ions are not confined to their two standard orientations found in K_3C_{60}. As the Na^+ ionic radius (0.95 Å) is smaller than the size of the hole, there is evidently enough space for the C_{60}^{3-} ions to rotate in such a way as to optimize both the attractive Na^+–C_{60}^{3-} interactions and the C_{60}^{3-}–C_{60}^{3-} contacts. The resulting structure is fcc, but differs from that of merohedrally disordered fullerides with respect to the orientational state of the C_{60}^{3-} ions, which are now quasi-spherically disordered. On cooling, a phase transition occurs in the vicinity of room temperature to a primitive cubic structure (space group $Pa\bar{3}$). Optimization of the C_{60} orientations occurs for the same orientational state found in solid C_{60}, namely an anticlockwise rotation about [111] of $\sim 98^\circ$. For this setting, the C–C contacts are optimized as 6:6 fusions "nest" over pentagonal faces of neighboring ions and at the same time, the Na^+–C_{60} coordination is highly optimal, as each C_{60} presents two hexagonal faces and six 6:6 fusions to its eight neighboring Na^+ ions, reducing their coordination number to 12.

The primitive cubic family of $Na_2(A, A')C_{60}$ ($A, A' =$ K, Rb, Cs) salts displays a much steeper rate of change of T_c with interfullerene spacing than that exhibited by the merohedrally disordered fcc fullerides (16), while at the same time, the effects of physical and chemical pressure on the superconducting properties are very different; chemical pressure suppresses T_c much faster than physical pressure does (Fig. 2) (17, 18). The origin of the faster depression of T_c with decreasing interfullerene separation in $Na_2(A, A')C_{60}$ is of particular interest. Empirically, it appears that the modified structure and intermolecular potential sensitively affect the electronic and conducting properties. The changed orientational state of the ions in the $Pa\bar{3}$ structures could affect electron hopping between neighboring ions and, as a consequence, might lead to a modified rate of change of $N(\varepsilon_F)$, and hence of T_c, with interfullerene spacing. However, the accumulated experimental evidence suggests that there is little difference in the a-dependence of $N(\varepsilon_F)$ between Na_2CsC_{60} ($Pa\bar{3}$) and K_3C_{60} and Rb_3C_{60} ($Fm\bar{3}m$) (19).

Subsequent experiments have revealed a more complicated situation than hitherto appreciated. The properties of ternary, Na_2AC_{60} and quaternary, $Na_2(A, A')C_{60}$ fullerides are highly sensitive to the cooling protocol. While upon rapid cooling, the salts remain strictly cubic, slow cooling stabilizes a monoclinic phase, comprising quasi-one-dimensional (1D) C_{60}^{3-} chains with short interball center-to-center

distances of 9.38 Å and bridged by single C–C bonds (Fig. 4) (20). The influence of the formation of the polymer on the superconducting properties is profound. Magnetization measurements were performed on Na_2RbC_{60} and Na_2CsC_{60} following different cooling procedures. The diamagnetic response in Na_2RbC_{60} is strongly suppressed on slow cooling, revealing that the polymer phase is not superconducting and that the observed superconducting fraction arises from the untransformed cubic phase. The situation is different for Na_2CsC_{60} which is completely insensitive to thermal history and remains strictly cubic. It thus appears that polymer formation occurs only below a critical interball separation. As far as the electronic properties of the Na_2AC_{60} polymers are concerned, they are found to be metallic. At small interchain separations ($A = Rb$), they remain conducting down to 4 K and show no instabilities, like the formation of SDW or CDW states. However, when the interchain separation is increased by gradual substitution of Rb by Cs across the series $Na_2Rb_{1-x}Cs_xC_{60}$, the increased one-dimensionality results in a transition to an AF insulating ground state below 45 K (21).

While superconductivity in sodium fullerides is confined to the isotropic 3D phases, there may be a connection between the suppressed values of T_c and polymer formation through the presence of intergrowths of non-superconducting polymer domains whose size grows as the lattice constant decreases. Such an interpretation is reminiscent of the detrimental effect on superconductivity of the formation of the LTT structure in the Ba-rich phases of the $La_{1.875}(Ba,Sr)_{0.125}CuO_4$ series. Although this is an appealing interpretation of the anomalous behavior of T_c, a number of additional Na-specific explanations still remain. These include: (i) the existence of an, as yet, unidentified low-symmetry distortion of the primitive cubic structure; (ii) a very sensitive modulation of the degree of electron transfer between Na and C_{60} by the interfullerene separation which leads to non-rigid band behavior, deviations from half filling of the conduction band and rapid suppression of superconductivity, in analogy with the situation encountered in non-superconducting Li_2CsC_{60} (*vide infra*). This analogy is reinforced by the observation that the high temperature fcc phase of Na_2CsC_{60} in which there is a clear evidence of Na^+–C interactions is insulating; and (iii) following the observation of dynamic Jahn–Teller distortions in Na_2CsC_{60} and charge fluctuations which create C_{60}^{2-} and C_{60}^{4-} ions (22), the light Na^+ ions can respond more easily to the higher electronic density regions in the primitive cubic structure, modifying the electronic/vibrational properties of the fulleride ions to such an extent, that superconductivity disappears.

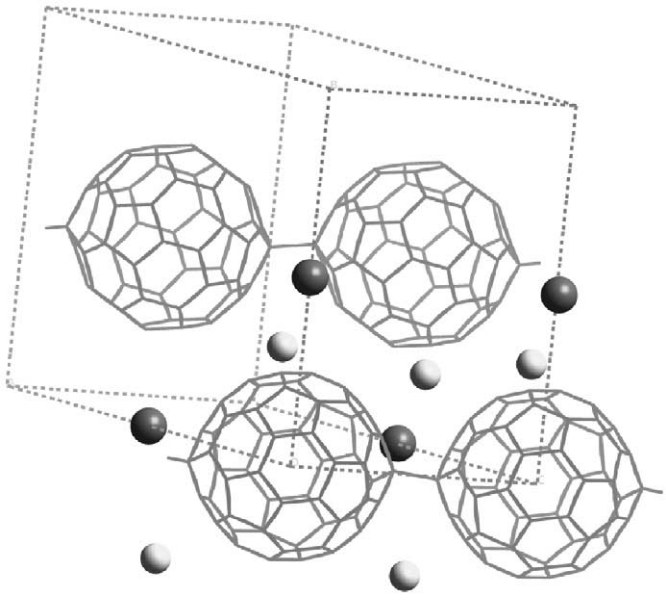

FIG. 4. Crystal structure of the Na_2RbC_{60} polymer (Na^+ ions are depicted as light-shaded spheres and Rb^+ ones as dark-shaded).

2.2.2. Lithium Fullerides

The synthesis of single-phase ternary Li fullerides, Li_2RbC_{60} and Li_2CsC_{60} was originally reported by Tanigaki *et al.* (23). These systems adopt an fcc structure at room temperature. Originally, SQUID measurements revealed the existence of a small diamagnetic fraction at low temperatures, possibly associated with an impurity phase. Li_2CsC_{60} seemed to have a T_c of 12 K with a shielding fraction of 1%. Subsequently, better characterized samples showed that both Li_2CsC_{60} and Li_2RbC_{60} are not superconductors, thus not obeying the simple monotonic relation between T_c and the lattice constant (Fig. 2). The non-superconducting properties can be related to the enhanced interactions between Li and C_{60} that modify the electronic structure at the Fermi level through partial hybridization of carbon p_z and metal 2*s* orbitals. Crystallographic analysis has revealed that an fcc structure comprising spherically disordered C_{60}^{3-} ions is adopted even at low temperatures (24). A symmetry-adapted spherical harmonics (SASH) analysis of the disordered C_{60}^{3-} ions reveals excess carbon density along the $\langle 1\,1\,1 \rangle$ direction, indicative of the Li^+–C interaction. As a result, the formal charge of the C_{60}^{n-} ions is less than 3, implying a less than half-full t_{1u} band and suppression of superconductivity. Raman measurements have established a value of the effective doping level, $n \approx 2.5$.

2.2.3. Dependence of Superconductivity on Band Filling

The disappearance of superconductivity in the Li-containing compounds has been rationalized in terms of

the strong lithium–carbon interaction discussed before. In order to overcome the Li^+–C interactions and achieve half-filling ($n = 3$) of the t_{1u} band, the series of fulleride salts, Li_xCsC_{60} ($1.5 < x < 6$) was synthesized (25). By adjusting the Li content, x, the electron transfer from the alkali metals to C_{60} and the filling level of the conduction band can be controlled (Fig. 5). Half filling was achieved for the composition Li_3CsC_{60} which is a bulk superconductor with $T_c = 10.5$ K. It is clear that superconductivity of the Li_xCsC_{60} salts is greatly suppressed as the band filling deviates from $n = 3$ towards both under- and over-doped directions. This is in excellent agreement with similar results on $Na_2Cs_xC_{60}$ ($0 < x < 1$) and $M_{3-y}Ba_yC_{60}$ ($0.2 < y < 2$; $M = K, Rb, Cs$) (26). For those series, a rapid decrease in T_c was also found both as n decreased below 3 ($T_c = 0.5$ K, $n = 2.5$, $Na_2Cs_{0.5}C_{60}$) and as n increased above 3. At low temperatures, Li_3CsC_{60} is primitive cubic (space group $Pa\bar{3}$), isostructural with the Na_2AC_{60} phases with orientationally ordered C_{60}^{3-} ions in the unit-cell (27). The tetrahedral and octahedral interstices are occupied by Li and Cs, respectively, while the excess Li (one per C_{60} unit) is disordered at the corners of a $(Li_8)_{1/8}$ cube with an edge length of ~ 3.4 Å, centered at the octahedral sites (Fig. 6). No anomalous close contacts between either the alkali metal ions or between Li^+ and the C_{60} units are encountered. The observed geometry of the Li defect is consistent with the existence of additional overdoped Li_xCsC_{60} phases with x between 4 and 6. On heating to room temperature, a phase transition occurs to fcc (space group $Fm\bar{3}m$) with orientationally disordered C_{60}^{3-} ions. The geometry of the Li^+ defect is unaffected by this phase change. The importance of the Li^+–C interactions in sensitively controlling the structural, conducting and electronic properties of lithium fullerides is clearly evident, while the rapid decrease of T_c as the C_{60} oxidation state deviates from -3 provides a stringent test for any theory of superconductivity in the fullerides.

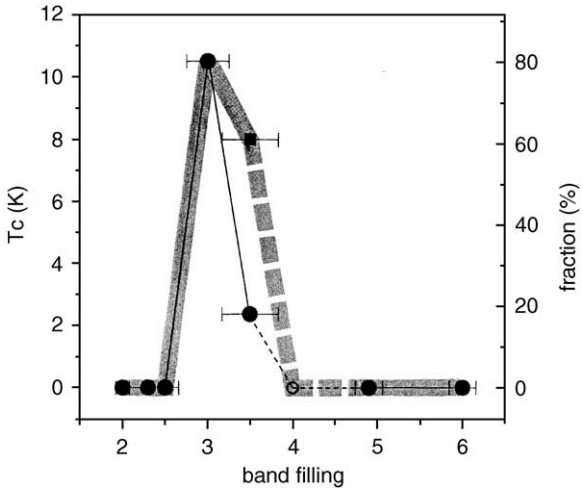

FIG. 5. Dependence of T_c (squares) and superconducting fractions (solid circles) of the Li_xCsC_{60} samples on the estimated filling of the C_{60} t_{1u} band. The datum for $n = 4$ ($KBaCsC_{60}$) is taken from Ref. (26) (open circle).

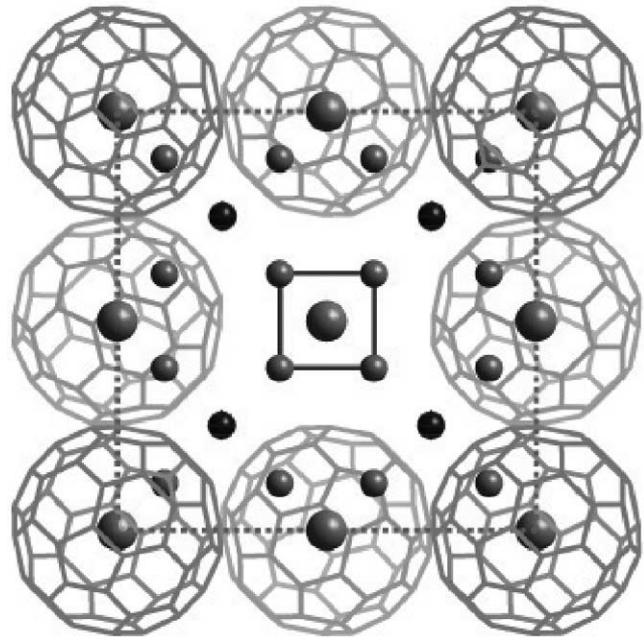

FIG. 6. Unit-cell basal plane projection of the primitive cubic Li_3CsC_{60} structure at low temperatures. The C_{60} units at the center of the (1 1 0) face have been removed for clarity.

2.3. Alkali Fullerides with Large Interfullerene Separations

2.3.1. Ammoniated Alkali Fullerides

An important issue in fullerene superconductivity, related to the correlation between T_c and interfullerene separation, depicted in Fig. 2, is the search for new materials with large lattice parameters in order to address the issue of whether these will be superconducting with increased T_c or the expected band narrowing at these interfullerene distances will lead to electron localization and a transition to a Mott insulating state. While the on-site interelectronic repulsion, U is a molecular quantity and does not vary in the A_3C_{60} series, the width of the t_{1u} conduction band, W depends sensitively on the interfullerene separation and the ratio (U/W) increases with increasing lattice constant. As a result, for large enough interball separations, (U/W) may exceed the critical value of 2.5 predicted by theory (10, 28) for the transition to an insulating state. An excellent method to synthesize such systems is to use as structural spacers alkali ions solvated with neutral molecules, such as ammonia. The NH_3 molecules coordinate to the alkali metal ions leading to

large effective radii for the resulting $(NH_3)_xA^+$ species which reside in the interstitial sites of the fullerene structure, while the extent of charge transfer is maintained. An early success of this approach was the ammoniation of superconducting Na_2CsC_{60} ($T_c = 12$ K) to afford $(NH_3)_4Na_2CsC_{60}$ which retained a cubic structure and whose T_c increased to 29.6 K (29).

However, when K_3C_{60} is intercalated with NH_3 to afford $(NH_3)K_3C_{60}$, superconductivity at ambient pressure is suppressed (30). The interfullerene separation (10.57 Å) has now exceeded that in cubic $RbCs_2C_{60}$ (10.29 Å, $T_c = 33$ K) but the lattice expansion is found to be anisotropic and to be accompanied by a reduction in crystal symmetry from cubic to orthorhombic. The nature of the electronic state of $(NH_3)K_3C_{60}$ at low temperatures has been investigated extensively. Magnetic susceptibility, electron spin resonance, and ^{13}C NMR measurements revealed that a metal–insulator transition occurs below 40 K (31). Muon spin relaxation (μ^+SR) studies provided unambiguous evidence that this is accompanied by the development of antiferromagnetic (AF) long-range order (32) with the temperature evolution of the internal magnetic field below T_N following closely the behavior of a conventional 3D Heisenberg AF with a staggered moment, $\mu(0) \approx 0.7\ \mu_B$/molecule. These results were subsequently confirmed by ESR and NMR studies (33, 34). The emerging picture is then that $(NH_3)K_3C_{60}$ is a narrow-band metal at high temperatures but on cooling a transition to a magnetic insulating state occurs before the onset of superconductivity (Fig. 7). The suppression of superconductivity and the metal–insulator transition are thus associated with effects of magnetic origin, providing an intriguing analogy with the phenomenology in organic and high-T_c superconductors.

The proximity of $(NH_3)K_3C_{60}$ to a metal–insulator transition has been ascribed to the crystal symmetry lowering which lifts the degeneracy of the t_{1u} orbitals and decreases the critical value of the (U/W) ratio for the transition to the AF Mott insulating state (10). As the degeneracy of the t_{1u} orbitals is lifted, $(U/W)_c$ decreases from ~ 2.5 to ~ 1 and the electronic properties of $(NH_3)K_3C_{60}$ are drastically different from those of cubic fullerides with comparable interfullerene separations. This is aided by the increased interfullerene separation (substantially larger than the value of 10.05 Å found in K_3C_{60}) which reduces the bandwidth, W and increases further (U/W). Interestingly, recovery of superconductivity with $T_c = 28$ K was, however, reported in $(NH_3)K_3C_{60}$ at pressures > 1 GPa (Fig. 7) (35). Structural work at elevated pressures (36) has established that the superconducting phase still retains a strongly distorted orthorhombic structure. The lifting of the degeneracy of the t_{1u} orbitals is thus not enough to keep the system on the insulating side of the metal–insulator transition. The nearest-neighbor

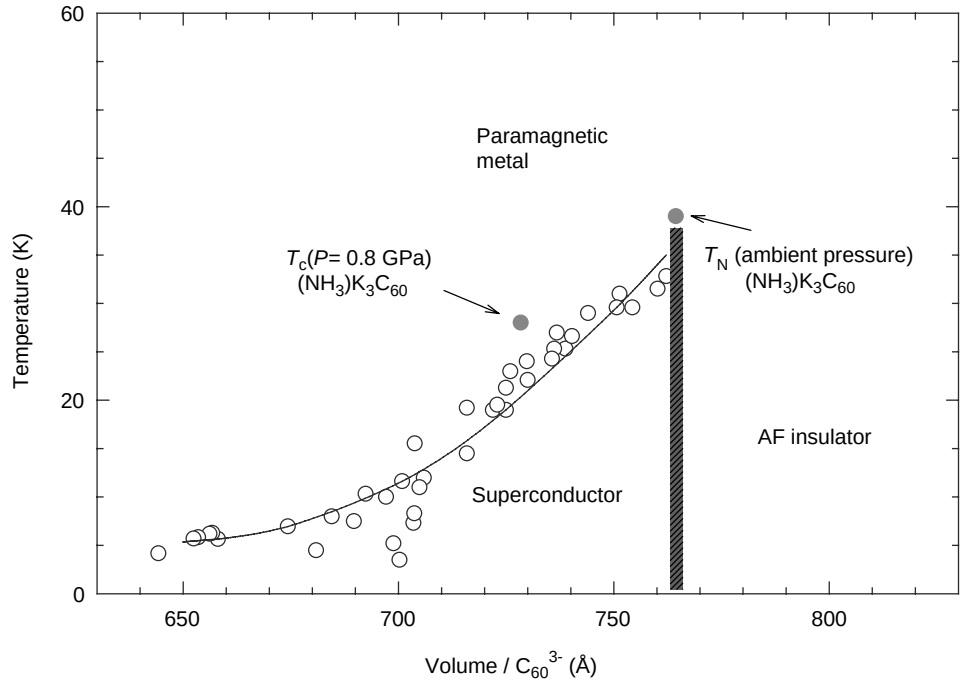

FIG. 7. Schematic electronic phase diagram of C_{60}^{3-} compounds, showing the approximate location of the metal (superconductor)–insulator phase boundary. The open symbols are literature values of T_c for a variety of superconducting fullerides, while the solid symbols mark T_N (ambient pressure) and T_c (> 1 GPa) of $(NH_3)K_3C_{60}$.

interfullerene separation in the *ab* plane shortens by $\sim 1.6\%$ between ambient pressure and 1.2 GPa. The resulting separation of 10.40 Å is comparable to that observed in the cubic $RbCs_2C_{60}$ fulleride and evidently leads to sufficient broadening of the conduction band to allow recovery of metallic behavior and superconductivity at 28 K. This behavior demonstrates beautifully the complex electronic properties of these highly correlated systems in which the metal–insulator transition can be studied over an unusually extended range of values of the bandwidth and the onsite interelectronic repulsion. We stress that the high pressure phase of $(NH_3)K_3C_{60}$ is the only non-cubic superconductor among the t_{1u}-based fullerides. Low-symmetry superconducting phases are more abundant among t_{1g}-based systems which are characterized by broader conduction bands and non-rigid band behavior arising from the strong mixing of metal and carbon orbitals (12).

Another prominent feature of fullerene-based materials is the sensitivity of their electronic and magnetic properties to orientational order/disorder of the C_{60} units which gives rise to different relative orientations of the molecular orbitals and different overlap of neighboring electronic wavefunctions. The relationship between the orientational, orbital and spin degrees of freedom has been theoretically explored for the $(TDAE)C_{60}$ ferromagnet (37). Indeed, it is reminiscent of the complex orbital, charge and magnetic order relationship encountered in strongly correlated transition metal oxides, like the CMR manganites (38). Interestingly, a structural phase transition has been observed in $(NH_3)K_3C_{60}$ below 150 K to an orthorhombic structure (space group *Fddd*) derived by doubling the lattice constants of the high temperature phase (space group *Fmmm*) along all three axes (39). The K^+–NH_3 pairs orient along the $\langle 1\,1\,0 \rangle$ direction in an antiferroelectric fashion, while the C_{60} units adopt two distinct orientations related by 90° about *c* and are antiferrorotatively ordered along *a* and *b* (Fig. 8) (40). There is a remarkable correlation of the C_{60} superstructure with the 3D AF structure and molecular orbital scheme proposed from NMR experiments (34) (Fig. 9). In the latter, the C_{60} units along [1 1 0] order antiferromagnetically, while those along [1 $\bar{1}$ 0] ferromagnetically. This implies that the nature of the intermolecular magnetic exchange interactions sensitively depends on the relative orientation of near-neighbor C_{60} units. Indeed, if one examines the nearest contacts between C_{60} along [110] and [1$\bar{1}$0], one finds that 6:5 C–C bonds face each other when viewed along the center-to-center direction but the existence of a center of inversion along [1 1 0] leads to pentagonal faces directed over hexagons and vice versa (40). On the other hand, along [1 $\bar{1}$ 0] pentagonal (hexagonal) faces of near-neighbors align over pentagons (hexagons). The observed ordering pattern is reminiscent of that proposed theoretically to account for the development of ferromagnetism in $(TDAE)C_{60}$ (37). The active role played by the C_{60} orientational degrees of freedom in the electronic and magnetic response of $(NH_3)K_3C_{60}$ is to a large extent reminiscent of the analogous strong coupling between the orbital, charge, spin and lattice responses in other strongly correlated systems like the manganese oxides (38).

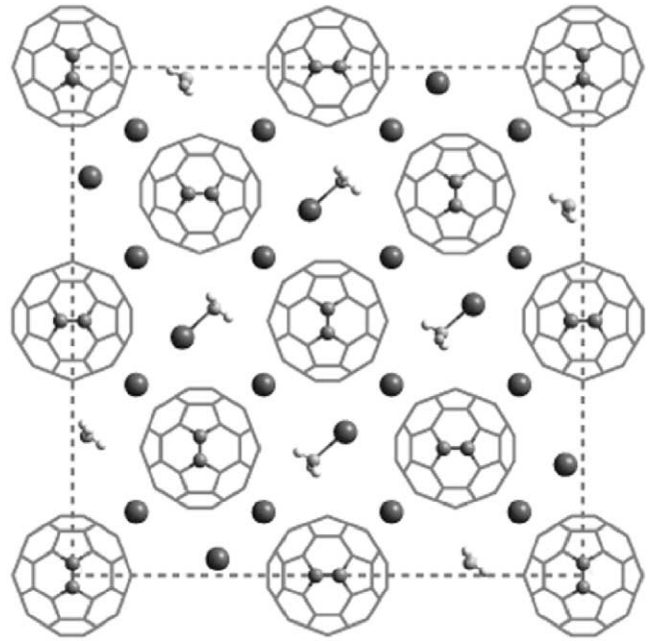

FIG. 8. Projection of the face-centered orthorhombic structure of $(NH_3)K_3C_{60}$ on the [1 1 0] basal plane. The ferrorotative (antiferrorotative) order of C_{60} along the base diagonal $\langle 1\,1\,0 \rangle$ ($\langle 1\,\bar{1}\,0 \rangle$) is shown.

Of particular interest are attempts to increase the interfullerene separation even further. For instance, the $(NH_3)K_{3-x}Rb_xC_{60}$ ($x = 1, 2, 3$) compounds are isostructural with $(NH_3)K_3C_{60}$ and also undergo an AF transition at low temperatures (41). The ordering temperature, T_N first increases with lattice expansion to 76 K for $x = 2$ and then decreases to 58 K for $x = 3$, in sharp contrast to what is expected for a simple localized moment model. Instead, the behavior is reminiscent of the phase diagram anticipated for a Mott–Hubbard system in which there is a crossover from itinerant to localized behavior with increasing (U/W) (i.e., increasing interfullerene separation).

2.3.2. *Breakdown of the Universal Dependence of T_c on Interfullerene Separation*

2.3.2.1. $A_xCs_{3-x}C_{60}$ fullerides. $RbCs_2C_{60}$ shows the highest T_c among cubic alkali fullerides at ambient pressure. Isolation of isostructural phases with stoichiometry $A_xCs_{3-x}C_{60}$ ($A = K, Rb$) and larger lattice constants

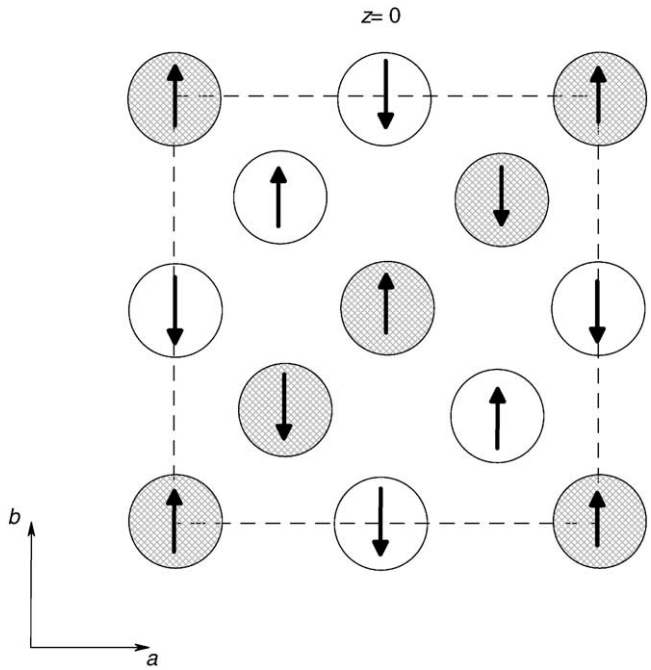

FIG. 9. Schematic diagram of orientational and magnetic order in the basal plane of the $(NH_3)K_3C_{60}$ structure. Shaded (open) circles denote orientation I (II) of C_{60}. The moment directions have yet to be determined and have been arbitrarily placed parallel to the *b*-axis.

than those of $RbCs_2C_{60}$ has led to the gradual suppression of T_c and a reversal of its expected dependence on interfullerene separation (42). In contrast to the ammoniated alkali fullerides, no transition is observed to an insulating state, a fact that can be associated with the retention of the degeneracy of the t_{1u} orbitals in these cubic fullerides. On the other hand, the decrease in T_c with decreasing bandwidth, W (and increasing U/W) may be rationalized in terms of the charge screening of the interelectronic repulsions within the t_{1u} conduction band (the renormalized Coulomb pseudopotential parameter, μ^* which appears in the McMillan equation). When $(U/W)<2$, μ^* is assumed to be ≈ 0.3 for the alkali fulleride superconductors. However, as the (U/W) ratio approaches the critical value for the Mott–Hubbard insulator transition (10), the screening becomes strongly inefficient and, in this part of the phase diagram, electron correlation effects (and μ^*) increase rapidly with increasing interfullerene separation leading to a different T_c dependence on the lattice constant from that "universally" encountered.

2.3.2.2. $(NH_3)_xNaA_2C_{60}$ fullerides. Quite puzzling are also the properties displayed by the series of superconducting ammoniated fullerides, $(NH_3)_xNaA_2C_{60}$ $(0.5<x<1$, $A = K, Rb)$ (43). In these systems, T_c is dramatically lower than expected from the universal curve and, in addition, it increases with decreasing ammonia content, x and decreasing lattice constant. Unlike the $(NH_3)K_3C_{60}$ family, there is no crystal symmetry reduction and the structure is fcc with merohedrally disordered C_{60}^{3-} units. Also unlike the $A_xCs_{3-x}C_{60}$ family, the interfullerene separation is not large enough to lead to sufficient band narrowing for superconductivity to be suppressed due to strong electron correlation effects. A possible rationale of the observed electronic properties may be associated with the geometry of the Na^+–NH_3 pairs which reside in the octahedral interstices. These are found to be disordered over the corners of two "interpenetrating" cubes centered at the octahedral holes with the Na^+ ions and the N atoms statically disordered over the corners of the inner and outer cube, respectively (Fig. 10) (44). The large off-centering of the Na^+ ion (~ 2.0 Å) could have detrimental effects on superconductivity as the C_{60}^{3-} units could experience a non-cubic local potential which should cause the lifting of the triple degeneracy of the LUMO and suppress the pairing mechanism. In addition, NH_3 loss along the series is accompanied by an increase of the metal content in the octahedral site which could reduce the effects of the local non-cubic crystal field and consequently, the shape of the conduction band should resemble more that of the conventional t_{1u} superconductors resulting in higher T_c. However, recent structural work has provided evidence of attractive N–$D\cdots\pi$ interactions between the $Na(NH_3)^+$ and the C_{60}^{3-} units (44) that may play a prominent role in determining the electronic properties of these systems.

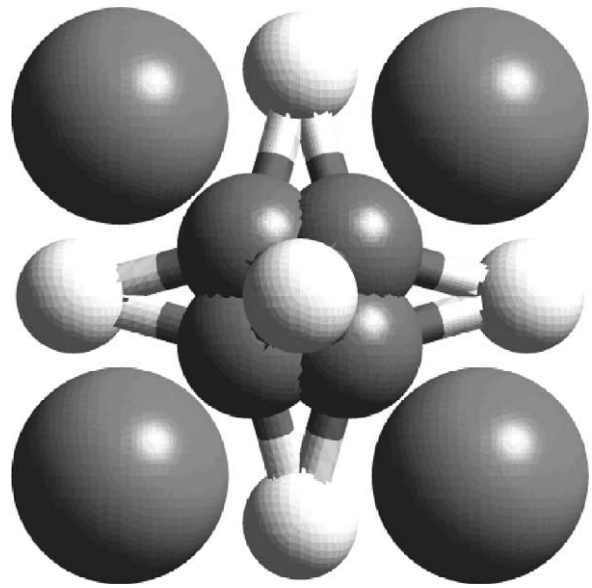

FIG. 10. Geometry of the disordered $Na(NH_3)^+$ unit residing in the octahedral holes of the $(NH_3)NaRb_2C_{60}$ structure. Large spheres are the Na^+ ions, small shaded and white spheres are the N and H atoms, respectively.

2.4. Alkaline- and Rare-Earth Fullerides

2.4.1. Alkaline-Earth Fullerides

The difficulty in synthesizing phase-pure alkaline earth fulleride samples made a systematic investigation of their properties rather challenging. However, due to the divalent character of these elements, the t_{1u}-derived band is now full, and occupation of the (LUMO + 1) t_{1g}-derived states occurs, opening the way to different energy scales and different criteria for the occurrence of superconductivity. Among the binary alkaline earth fullerides superconductivity is encountered for different compositions. Calcium forms a primitive cubic salt with stoichiometry Ca_5C_{60}, which becomes superconducting at 8.4 K (45). On the other hand, strontium and barium metals form stable compositions AE_xC_{60} for $x = 3$, 4, and 6. AE_3C_{60} (AE = Ba, Sr) are insulating and adopt the $A15$ structural type (space group $Pm\bar{3}n$) (46). It is noteworthy that this structural type is also adopted by Cs_3C_{60}, which is superconducting at $\sim$40 K at elevated pressures, the highest reported T_c for an electron doped fulleride superconductor (3).

The AE_6C_{60} ($AE = Ba, Sr$) phases have proven more controversial. Early work established their structures correctly as bcc (space group $Im\bar{3}$) but proposed they were superconducting with $T_c = 4$ K for Sr_6C_{60} and 6.5 K for Ba_6C_{60} (47). Subsequently, it was unambiguously established that both Sr_6C_{60} and Ba_6C_{60} are metallic despite the formally full t_{1g}-derived band, but not superconducting (48). The $N(\varepsilon_F)$ values of 5.6 and 9.5 states eV^{-1} (mol $C_{60})^{-1}$ for Ba_6C_{60} and Sr_6C_{60}, respectively, increase as the interfullerene separation decreases, a tendency opposite to that exhibited by the metallic alkali fullerides. This inverted trend was rationalized both theoretically (49) and experimentally (48) in terms of a strong hybridization between the alkaline earth d and s orbitals and C_{60} $p\pi$ orbital which leads to a modified and much broader conduction band.

The bulk superconducting phases in the Ba–C_{60} and Sr–C_{60} systems have been established unambiguously to have stoichiometries Ba_4C_{60} and Sr_4C_{60} with T_c of 6.7 and 4.4 K, respectively. These adopt a highly anisotropic orthorhombic structure (space group $Immm$) revealing a new structural criterion for the occurrence of superconductivity, as the fullerene superconductors identified so far had been limited to cubic or slightly distorted cubic structures. Accurate structural determination showed the existence of very short Ba–C contacts which imply strong hybridization between the 5d orbitals of Ba and the 2p orbitals of carbon (12). Such a strong orbital mixing was confirmed by LDA calculations (50). The occurrence of superconductivity in non-cubic Ba_4C_{60} is in sharp contrast with the absence of superconductivity in alkali fullerides, A_4C_{60} despite the similar (A = K, Rb) or identical (A = Cs) structures. In A_4C_{60}, the electrons are localized, most likely by the combined effect of electron correlation and electron–phonon interaction. Since the alkali fullerides are at the verge of the metal–insulator boundary, because of the narrow band nature of the t_{1u}-originated conduction band, distortion from cubic symmetry and deviation from half filling easily destroy the metallic state and, as a result, superconductivity. In AE_4C_{60} the metallic state is much more robust. In fact, $N(\varepsilon_F)$ is 6.0 and 2.5 states eV^{-1} (mol $C_{60})^{-1}$ for Ba_4C_{60} and Sr_4C_{60}, respectively, considerably smaller than those of the t_{1u}-superconductors, K_3C_{60} and Rb_3C_{60}, indicating broader conduction bands for the AE_4C_{60} systems. The structural and electronic properties of the alkaline-earth fullerides are dominated by the hybridization effects, which modify and increase the width of the conduction band leading to a stabilization of the metallic state.

The $A_3Ba_3C_{60}$ (A = K, Rb, Cs) family is also of particular interest, as the t_{1g} band is formally half full and the interfullerene separation can be controlled by the size of the alkali cation. Bulk superconductivity is observed for $K_3Ba_3C_{60}$ ($T_c = 5.6$ K) and $Rb_3Ba_3C_{60}$ ($T_c = 2.0$ K), while $Cs_3Ba_3C_{60}$ is not a superconductor down to 0.5 K. $N(\varepsilon_F)$ decreases with increasing cell size in sharp contrast with the A_3C_{60} superconductors (51). Structural analysis of body-centered cubic $K_3Ba_3C_{60}$ revealed the existence of short Ba–C and K–C contacts, implying hybridization between the K, Ba, and C_{60} states (52). The orbital mixing strongly modifies the shape of the conduction band, leading to a larger bandwidth and a smaller value of $N(\varepsilon_F)$ than those encountered in other t_{1u} superconductors, despite the similar band filling. In addition, the observation of local distortions in the distorted tetrahedral sites may be responsible for the observed complex relationship between T_c and cubic lattice parameter.

2.4.2. Rare-Earth Fullerides

Intercalation of C_{60} with rare-earth metals results in interesting compounds not only for the appearance of superconductivity but also for the magnetic properties related to the localized 4f electrons. Single phase compositions have been reported for stoichiometries R_xC_{60} with $x = 2.75$ and 6 (R = Yb, Sm, Eu). Superconductivity is observed for $Yb_{2.75}C_{60}$($T_c = 6$ K) and $Sm_{2.75}C_{60}$ (T_c = 8 K) where the metal atoms are divalent and non-magnetic (53). The Yb or Sm cations occupy off-centered interstitial sites in the fcc C_{60} lattice, and leave eight tetrahedral sites vacant in an orthorhombic unit-cell which is doubled in each direction. These cation-vacancy sites exhibit long-range ordering, generating a superstructure which is stabilized by a short-range interaction between charge-deficient single bonds in C_{60} and the divalent cations.

Recent work on the phase diagram of Eu–C_{60} has led to the isolation of the highly doped Eu_6C_{60} composition which is bcc and displays a transition to a ferromagnetic

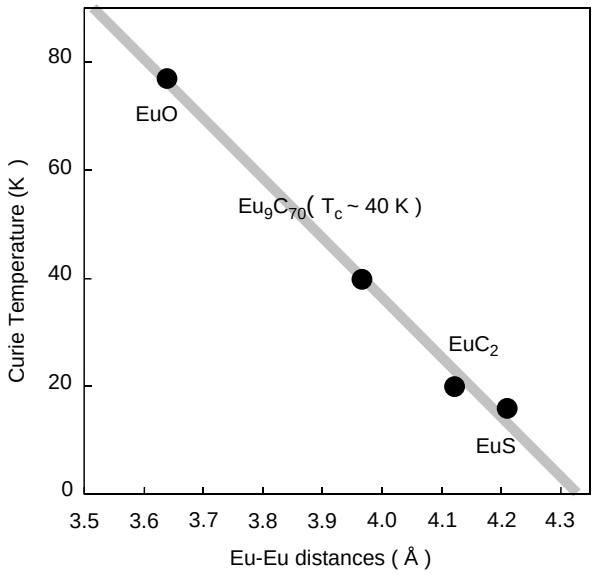

FIG. 11. Relationship between ferromagnetic transition temperature, T_C of Eu^{2+} compounds and nearest Eu–Eu distance.

state near $T_C = 14$ K (54). The Eu atoms are in the divalent state with a magnetic moment of 7.1(3) μ_B ($S = \frac{7}{2}$) (55) and there is evidence that the magnetic interactions are not purely of direct exchange nature, but are modulated through the C_{60} units. Highly doped Eu_9C_{70} is also a ferromagnet with a saturation magnetic moment of 7 μ_B and a high T_C of 40 K (56). The ferromagnetic interaction in NaCl-type semiconductors of Eu^{2+} is due to Eu^{2+} nearest-neighbor f–f interactions and T_C is modulated by the Eu^{2+}–Eu^{2+} distances. In Eu_9C_{70}, the shortest Eu–Eu distance is ~3.96 Å. A plot of T_C vs nearest-neighbor distance is shown in Fig. 11 with the T_C of Eu_9C_{70} scaling well and implying an identical magnetic exchange mechanism. For Eu_6C_{60}, the shortest Eu–Eu contact is ~3.87 Å but the value of T_C is lower than expected from a direct f–f interaction. As in the bcc Eu_6C_{60} structure, there is evidence of strong hybridization and orbital mixing between the metals and C_{60}, the magnetic exchange interaction between Eu^{2+} ions is modulated by C_{60} through p–f interactions.

3. FULLERENE SUPERCONDUCTIVITY IN FET DEVICES

The most spectacular advances in the study of the electronic properties of fullerene solids have come from the results obtained by doping fullerene single crystals in electronic devices called field-effect transistors (FET). In essence, a gate electrode is placed on top of an oxide (Al_2O_3) layer grown on the surface of a single crystal (e.g., C_{60}, C_{70}) to which source and drain electrodes have been also added. Charge carriers can be injected in the surface layer (2D doping) of the crystal by applying a voltage to the gate electrode—electrons are injected for a positive voltage, holes for a negative one. The level of doping can be tuned by changing the applied voltage and in this way, the electronic properties can be followed in a continuous fashion as a function of doping (hole or electron) over a wide range without the crystallographic changes that may accompany chemical doping.

The first success of this approach was the demonstration that electron-doping of pristine C_{60} can be induced in a FET device, leading to a T_c of 11 K at a doping level of ~3 electrons per molecule, close to half filling of the t_{1u} band (57). The superconducting region extends between 2.5 and 3.6 electrons per molecule in excellent agreement with what has been observed before in bulk intercalated fullerides. In addition, the observed $T_{c,max}$ is in agreement with the universal dependence of T_c on interfullerene separation in A_3C_{60} (Fig. 12). Even more importantly, it has been also possible to dope the surface of C_{60} with holes which because of the high electronegativity of C_{60} had not been achieved before by chemical means. Hole-doping of the h_u valence band (Fig. 1) is of interest as T_c is predicted to be even higher as a result of the increased density-of-states at the Fermi level, $N(\varepsilon_F)$ (higher orbital degeneracy of the HOMO) and the increased electron–phonon coupling strength (calculated to be 1.4 times larger) (58). Indeed experimentally $T_{c,max}$ jumps to 52 K at a doping level of ~3.2 holes per C_{60} with the superconducting region being wider and extending between 1.5 and 4.5 electrons per C_{60} (Fig. 13) (59). Interestingly in this case, $T_{c,max}$ does not coincide with a formally half-filled h_u-derived band.

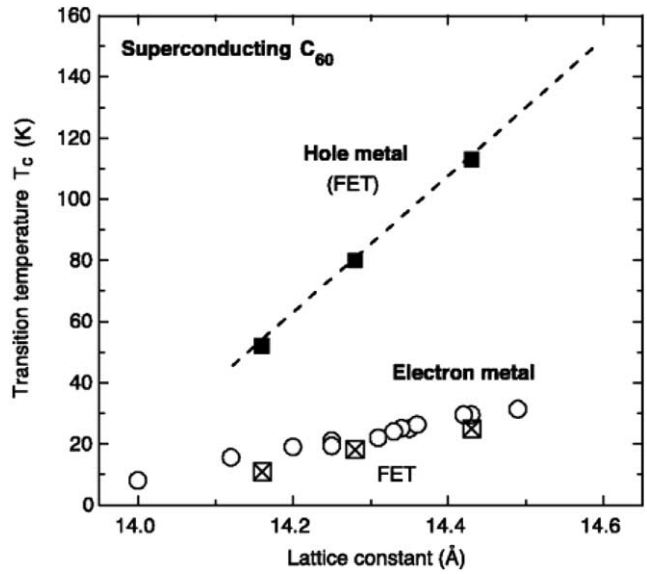

FIG. 12. Variation in T_c as a function of lattice constant for electron- and hole-doped C_{60} crystals. Square symbols are the results from FET experiments and open circles refer to A_3C_{60} fullerides. Reprinted with permission from *Science*, J. H. Schon, C. Kloc, and B. Batlogg, 293, 2432, Copyright 2001.

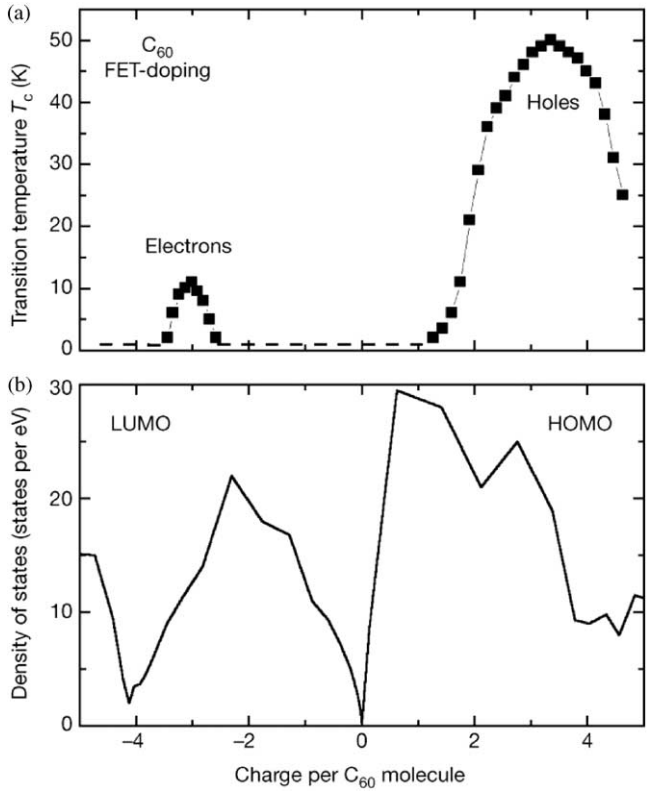

FIG. 13. T_c (a) and density-of-states (b) as a function of charge per C_{60} molecule. Reprinted with permission from *Nature*, J. H. Schon, C. Kloc, and B. Batlogg, 408, 549, Copyright 2000 Macmillan Publishers Ltd.

As discussed extensively earlier, increasing the interfullerene separation drives T_c higher, as $N(\varepsilon_F)$ rapidly increases. In accordance with this, gate-induced superconductivity in hole-doped co-crystals of $C_{60}/CHCl_3$ and $C_{60}/CHBr_3$ approaches onset values of 83 and 117 K, respectively, as the interfullerene separation increases from 10.01 Å in pristine C_{60} to 10.10 and 10.20 Å in $C_{60}/CHCl_3$ and $C_{60}/CHBr_3$, respectively (Fig. 12) (5). The observed T_c's are only surpassed by the high-T_c cuprates. Further, even small, expansion of the interfullerene separation should allow transition temperatures in excess of 150 K to be achieved, before the effects of electron correlation become dominant and a transition to an insulating state occurs in analogy with the behavior of bulk intercalated fullerides.

Observation of these spectacularly high-T_c's in simple non-metal-containing systems represents a milestone for the field of superconductivity. They are certainly higher than anything that was thought possible for phonon-driven superconductivity. If phonons prove to be important here, then phononic mechanisms of superconductivity should be reconsidered even for the cuprates. It may be that non-adiabatic effects arising from the comparable energy scales of the Fermi and phonon energies in these narrow band metals could be important (60). Alternatively, electronic mechanisms could be responsible for providing the high-temperature superconducting pairing (61). In any case, continuous gate-induced 2D doping of C_{60} should allow for a systematic understanding of the electronic properties of these fascinating materials. In addition, it will provide comparisons with the electronic behavior of bulk 3D chemically intercalated fullerides.

4. NON-C_{60} FULLERENES

Till now, attempts to synthesize superconducting salts of fullerenes other than C_{60} have been unsuccessful. Higher fullerenes (C_{70}, C_{84}) have lower molecular symmetry than C_{60} resulting in the removal of the triple orbital degeneracy of the LUMO which should result in lower values of $N(\varepsilon_F)$ in their metallic salts and lower T_c's. In addition, the electron–phonon coupling strength, V is expected to decrease with decreasing curvature of the fullerene skeleton, as the sp^3 hybridization of the C orbitals will decrease and the contribution of the radial vibrational modes to V diminishes (8). This will also suppress T_c. Finally, their non-spherical shape also favors formation of crystalline salts with either non-cubic symmetry or with pronounced static orientational disorder of the fulleride units and/or positional disorder of the intercalated ions, factors which enhance the possibility of electron localization. Recent experiments on electron-doping of a single crystal of C_{70} using an FET device have demonstrated that there is no intrinsic reason for superconductivity not to occur in a higher fullerene at the appropriate doping level. Gate-induced superconductivity was observed at 7 K for $\sim$4 electrons per C_{70}, corresponding to half filling of the conduction band (62).

This implies that the search for higher T_c in the fullerene family could be extended to solid phases of smaller fullerenes, like C_{28} and C_{36} which should be characterized by larger electron–phonon coupling strengths, associated with their increased curvatures (8, 63). Finally, we note that superconductivity was reported in 4 Å single wall carbon nanotubes embedded in a zeolite matrix (64).

5. CONCLUSION

Work on the condensed phases of fullerenes and their derivatives continues to lead to unexpected results whose significance extends to other areas of solid-state chemistry and physics. Unlike in other superconducting materials, the key ingredients in the mechanism of superconductivity, namely the electron–phonon coupling strength (an intramolecular property) and the density-of-states at the Fermi level (an intermolecular property) are decoupled. This has allowed the exploration of a large parameter space in a systematic manner by structurally modulating $N(\varepsilon_F)$, while keeping V essentially fixed. At small interfullerene separa-

tions, metal–C_{60} interactions become increasingly important leading to non-rigid band behavior. At the same time, C_{60}–C_{60} bond formation also competes with the monomer phases, leading to a variety of low-dimensional architectures with interesting electronic properties. At large fullerene spacings, the highly correlated narrow-band character of the metallic phases leads to rich physical behavior and the competition with magnetic insulating phases, in analogy with other classes of superconducting materials. Finally, the development of the FET channel of electron- and hole-doping technique has led to unprecedented high T_c in these organic superconductors, prompting a broad reconsideration of mechanisms which can provide high-temperature superconducting pairing.

ACKNOWLEDGMENTS

S.M. thanks Jesus College, Cambridge for a Research Fellowship. We acknowledge a long-standing collaboration with Prof. Y. Iwasa (Tohoku) and financial support by the NEDO FCT program.

REFERENCES

1. O. Gunnarsson, *Rev. Mod. Phys.* **69,** 575 (1997); K. Prassides, *Curr. Opin. Solid State Mater. Sci.* **2,** 433 (1997); M. J. Rosseinsky, *Chem. Mater.* **10,** 2665 (1998); W. Andreoni, "The Physics of Fullerene-Based and Fullerene-Related Materials." Kluwer Academic Publishers, Dordrecht, 2000; K. M. Kadish and R. S. Ruoff, "Fullerenes. Chemistry, Physics, and Technology." Wiley/Interscience, New York, 2000; L. Mihaly and L. Forro, *Rep. Prog. Phys.* **64,** 649 (2001).
2. K. Tanigaki, T. W. Ebbesen, S. Saito, J. Mizuki, J. S. Tsai, Y. Kubo, and S. Kuroshima, *Nature* **352,** 222 (1991).
3. T. T. M. Palstra, O. Zhou, Y. Iwasa, P. E. Sulewski, R. M. Fleming, and B. R. Zegarski, *Solid State Commun.* **93,** 327 (1995).
4. R. M. Fleming, A. P. Ramirez, M. J. Rosseinsky, D. W. Murphy, R. C. Haddon, S. M. Zahurak, and A. V. Makhija, *Nature* **352,** 787 (1991).
5. J. H. Schon, C. Kloc, and B. Batlogg, *Science* **293,** 2432 (2001).
6. P. M. Allemand, K. C. Khemani, A. Koch, F. Wudl, K. Holczer, S. Donovan, G. Gruner, and J. D. Thompson, *Science* **253,** 301 (1991).
7. T. L. Makarova, B. Sundqvist, R. Hohne, P. Esquinazi, Y. Kopelevich, P. Scharff, V. A. Davydov, L. S. Kashevarova, and A. V. Rakhmanina, *Nature* **413,** 716 (2001).
8. M. Schluter, M. Lannoo, M. Needles, and G. A. Baraff, *Phys. Rev. Lett.* **68,** 526 (1992).
9. S. Chakravarty, M. P. Gelfand, and S. Kivelson, *Science* **254,** 970 (1991).
10. E. Koch, O. Gunnarsson, and R. M. Martin, *Phys. Rev. Lett.* **83,** 620 (1999).
11. R. W. Lof, M. A. VanVeenendaal, B. Koopmans, H. T. Jonkman, and G. A. Sawatzky, *Phys. Rev. Lett.* **68,** 3924 (1992).
12. C. M. Brown, S. Taga, B. Gogia, K. Kordatos, S. Margadonna, K. Prassides, Y. Iwasa, K. Tanigaki, A. N. Fitch, and P. Pattison, *Phys. Rev. Lett.* **83,** 2258 (1999).
13. P. W. Stephens, L. Mihaly, P. L. Lee, R. L. Whetten, S. M. Huang, R. Kaner, F. Deiderich, and K. Holczer, *Nature* **351,** 632 (1991).
14. R. E. Walstedt, D. W. Murphy, and M. J. Rosseinsky, *Nature* **362,** 611 (1993).
15. J. E. Fischer, G. Bendele, R. Dinnebier, P. W. Stephens, C. L. Lin, N. Bykovetz, and Q. Zhu, *J. Phys. Chem. Solids* **56,** 1445 (1995).
16. K. Prassides, C. Christides, I. M. Thomas, J. Mizuki, K. Tanigaki, I. Hirosawa, and T. W. Ebbesen, *Science* **263,** 950 (1994).
17. T. Yildirim, J. E. Fischer, R. Dinnebier, P. W. Stephens, and C. L. Lin, *Solid State Commun.* **93,** 269 (1995).
18. C. M. Brown, T. Takenobu, K. Kordatos, K. Prassides, Y. Iwasa, and K. Tanigaki, *Phys. Rev. B* **59,** 4439 (1999).
19. K. Tanigaki and K. Prassides, *J. Mater. Chem.* **5,** 1515 (1995); P. Petit and J. Robert, *Appl. Magn. Reson.* **11,** 183 (1996).
20. K. Prassides, K. Vavekis, K. Kordatos, K. Tanigaki, G. M. Bendele, and P. W. Stephens, *J. Am. Chem. Soc.* **119,** 834 (1997); G. M. Bendele, P. W. Stephens, K. Prassides, K. Vavekis, K. Kordatos, and K. Tanigaki, *Phys. Rev. Lett.* **80,** 736 (1998).
21. D. Arcon, K. Prassides, A.-L. Maniero, and L. C. Brunel, *Phys. Rev. Lett.* **84,** 562 (2000); F. Simon, S. Garaj, and L. Forro, *Phys. Rev. Lett.* **87,** 129,703 (2001); D. Arcon, K. Prassides, A.-L. Maniero, and L. C. Brunel, *Phys. Rev. Lett.* **87,** 129,704 (2001).
22. V. Brouet, H. Alloul, T.-N. Le, S. Garaj, and L. Forro, *Phys. Rev. Lett.* **86,** 4680 (2001).
23. K. Tanigaki, I. Hirosawa, T. W. Ebbesen, J. Mizuki, Y. Shimakawa, Y. Kubo, J. S. Tsai, and S. Kuroshima, *Nature* **356,** 419 (1992).
24. I. Hirosawa, K. Prassides, J. Mizuki, K. Tanigaki, M. Gevaert, A. Lappas, and J. K. Cockcroft, *Science* **264,** 1294 (1994).
25. M. Kosaka, K. Tanigaki, K. Prassides, S. Margadonna, C. M. Brown, A. Lappas, and A. N. Fitch, *Phys. Rev. B* **59,** R6628 (1999).
26. T. Yildirim, L. Barbedette, J. E. Fischer, C. L. Lin, J. Robert, P. Petit, and T. T. M. Palstra, *Phys. Rev. Lett.* **77,** 1167 (1996).
27. S. Margadonna, K. Prassides, A. N. Fitch, M. Kosaka, and K. Tanigaki, *J. Am. Chem. Soc.* **121,** 6318 (1999).
28. O. Gunnarsson, E. Koch, and R. M. Martin, *Phys. Rev. B* **54,** R11026 (1996).
29. O. Zhou, R. M. Fleming, D. W. Murphy, M. J. Rosseinsky, A. P. Ramirez, R. B. van Dover, and R. C. Haddon, *Nature* **362,** 433 (1993).
30. M. J. Rosseinsky, D. W. Murphy, R. M. Fleming, and O. Zhou, *Nature* **364,** 425 (1993).
31. Y. Iwasa, H. Shimoda, T. T. M. Palstra, Y. Maniwa, O. Zhou, and T. Mitani, *Phys. Rev. B* **53,** R8836 (1996); K. M. Allen, S. J. Heyes, and M. J. Rosseinsky, *J. Mater. Chem.* **6,** 1445 (1996).
32. K. Prassides, S. Margadonna, D. Arcon, A. Lappas, H. Shimoda, and Y. Iwasa, *J. Am. Chem. Soc.* **121,** 11,227 (1999).
33. F. Simon, A. Janossy, F. Muranyi, T. Feher, H. Shimoda, Y. Iwasa, and L. Forro, *Phys. Rev. B* **61,** R3826 (2000).
34. H. Tou, Y. Maniwa, Y. Iwasa, H. Shimoda, and T. Mitani, *Phys. Rev. B* **62,** R775 (2000).
35. O. Zhou, T. T. M. Palstra, Y. Iwasa, R. M. Fleming, A. F. Hebard, P. E. Sulewski, D. W. Murphy, and B. R. Zegarski, *Phys. Rev. B* **52,** 483 (1995).
36. S. Margadonna, K. Prassides, H. Shimoda, Y. Iwasa, and M. Mezouar, *Europhys. Lett.* **56,** 61 (2001).
37. K. Tanaka, Y. Asai, T. Sato, T. Kuga, T. Yamabe, and M. Tokumoto, *Chem. Phys. Lett.* **259,** 574 (1996); T. Kawamoto, *Solid State. Commun.* **101,** 231 (1997).
38. Y. Tokura and N. Nagaosa, *Science* **288,** 462 (2000).
39. K. Ishii, T. Watanuki, A. Fujiwara, H. Suematsu, Y. Iwasa, H. Shimoda, T. Mitani, H. Nakao, Y. Fujii, Y. Murakami, and H. Kawada, *Phys. Rev. B* **59,** 3956 (1999).
40. S. Margadonna, K. Prassides, H. Shimoda, T. Takenobu, and Y. Iwasa, *Phys. Rev. B* **64,** 132,414 (2001).

41. T. Takenobu, T. Muro, Y. Iwasa, and T. Mitani, *Phys. Rev. Lett.* **85,** 381 (2000).
42. P. Dahlke, M. S. Denning, P. F. Henry, and M. J. Rosseinsky, *J. Am. Chem. Soc.* **122,** 12,352 (2000).
43. H. Shimoda, Y. Iwasa, Y. Miyamoto, Y. Maniwa, and T. Mitani, *Phys. Rev. B* **54,** R15653 (1996).
44. S. Margadonna, E. Aslanis, and K. Prassides, *J. Am. Chem. Soc.* **124,** 10146 (2002).
45. A. R. Kortan, N. Kopylov, S. Glarum, E. M. Gyorgy, A. P. Ramirez, R. M. Fleming, F. A. Thiel, and R. C. Haddon, *Nature* **355,** 529 (1992).
46. A. R. Kortan, N. Kopylov, R. M. Fleming, O. Zhou, F. A. Thiel, R. C. Haddon, and K. M. Rabe, *Phys. Rev. B* **47,** 13,070 (1993).
47. A. R. Kortan, N. Kopylov, S. Glarum, E. M. Gyorgy, A. P. Ramirez, R. M. Fleming, O. Zhou, F. A. Thiel, P. L. Trevor, and R. C. Haddon, *Nature* **360,** 566 (1992).
48. B. Gogia, K. Kordatos, H. Suematsu, K. Tanigaki, and K. Prassides, *Phys. Rev. B* **58,** 1077 (1998).
49. S. Saito and A. Oshiyama, *Phys. Rev. Lett.* **71,** 121 (1993).
50. K. Umemoto and S. Saito, *Phys. Rev. B* **61,** 14,204 (2000).
51. Y. Iwasa, H. Hayashi, T. Furudate, and T. Mitani, *Phys. Rev. B* **54,** 14,960 (1996); Y. Iwasa, M. Kawaguchi, H. Iwasaki, T. Mitani, N. Wada, and T. Hasegawa, *Phys. Rev. B* **57,** 13,395 (1998).
52. S. Margadonna, E. Aslanis, W. Z. Li, K. Prassides, A. N. Fitch, and T. C. Hansen, *Chem. Mater.* **12,** 2736 (2000).
53. E. Ozdas, A. R. Kortan, N. Kopylov, A. P. Ramirez, T. Siegrist, K. M. Rabe, H. E. Bair, S. Schuppler, and P. H. Citrin, *Nature* **375,** 126 (1995); X. H. Chen and G. Roth, *Phys. Rev. B* **52,** 15,534 (1995).
54. H. Ootoshi, K. Ishii, A. Fujiwara, T. Watanuki, Y. Matsuoka, and H. Suematsu, *Mol. Cryst. Liq. Cryst.* **340,** 565 (2000).
55. I. Margiolaki, S. Margadonna, K. Prassides, K. Ishii, H. Suematsu, and T. Hansen, *J. Am. Chem. Soc.* **124,** 11288 (2002).
56. T. Takenobu, D. H. Chi, S. Margadonna, K. Prassides, Y. Kubozono, A. N. Fitch, K. Kato, and Y. Iwasa, *J. Am. Chem. Soc.*, submitted.
57. J. H. Schon, C. Kloc, R. C. Haddon, and B. Batlogg, *Science* **288,** 656 (2000).
58. I. I. Mazin, S. N. Rashkeev, V. P. Antropov, O. Jepsen, A. I. Liechtenstein, and O. K. Andersen, *Phys. Rev. B* **45,** 5114 (1992); N. Manini, A. Dal Corso, M. Fabrizio, and E. Tosatti, *Philos. Mag. B* **81,** 793 (2001).
59. J. H. Schon, C. Kloc, and B. Batlogg, *Nature* **408,** 549 (2000).
60. E. Cappelluti, C. Grimaldi, and L. Pietronero, *Phys. Rev. B* **64,** 125,104 (2001).
61. S. Chakravarty and S. A. Kivelson, *Phys. Rev. B* **64,** 064,511 (2001).
62. J. H. Schon, C. Kloc, T. Siegrist, M. Steigerwald, C. Svensson, and B. Batlogg, *Nature* **413,** 831 (2001).
63. N. Breda, R. A. Broglia, G. Colo, G. Onida, D. Provasi, and E. Vigezzi, *Phys. Rev. B* **62,** 130 (2000).
64. Z. K. Tang, L. Y. Zhang, N. Wang, X. X. Zhang, G. H. Wen, G. D. Li, J. N. Wang, C. T. Chan, and P. Sheng, *Science* **292,** 2462 (2001).